Applied Catalysis A, General 707 (2025) 120536

Contents lists available at ScienceDirect

Applied Catalysis A, General

journal homepage: www.elsevier.com/locate/apcata

Surface modification of nanocatalysts via ion beam techniques for enhanced activity

Hanna Solt [a], Marina Maddaloni [g], Philippe Bazin [a], Damien Aureau [b], Arnaud Etcheberry [b], Denis Busardo [c], Séverine Rousseau [d], Gilbert Blanchard [d], Najat Moral [e], Alina Bruma [f], Sylvie Malo [f], Marco Daturi [a], Nancy Artioli [g,*]

[a] Laboratoire Catalyse et Spectrochimie, ENSICAEN, Université de Caen, CNRS, 6 Bd Maréchal Juin, Caen 14050, France
[b] IREM-Institut Lavoisier, 45 rue des Etats-Unis, Versailles Cedex 78035, France
[c] Scientific Director, Quertech, 9 rue de la Girafe, Caen 14000, France
[d] PSA Peugeot Citroën – Centre Technique de la Garenne-Colombes, 18 Rue des Fauvelles – Mail Box LG084, Colombes, La Garenne 92256, France
[e] Renault Automobiles, Centre Technique de Lardy, 1 Allée de Cornuel, Lardy 91510, France
[f] CRISMAT, UMR CNRS ENSICAEN 6508, 6 bd Maréchal Juin, Caen Cedex 4 14050, France
[g] CEEP Laboratory, Department of Civil Engineering, Architecture, Territory, Environment and Mathematics, University of Brescia, Via Branze 38, Brescia 25123, Italy

ARTICLE INFO

Keywords:
Ion
Bombardment
Nanocatalyts
DOC catalystsCeZrO2

ABSTRACT

Interface science is at the forefront of advanced materials design, particularly in catalysis, where surface properties critically determine performance. Among emerging techniques, ion beam irradiation has shown strong potential for modifying the catalytic behavior of solid materials by introducing surface and sub-surface defects. In this study, the effect of nitrogen ion irradiation on the catalytic and redox properties of a ceria–zirconia-based oxidation catalyst ($Ce_{0.68}Zr_{0.32}O_2$), both in its unmodified form and when combined with supported Pt nanoparticles, was systematically investigated through a series of catalytic tests (TPO/TPR), operando FTIR, HRTEM, and XPS analyses. Ion bombardment was found to induce significant modifications to nanoparticle distribution, surface morphology, and defect structure—most notably the formation of oxygen vacancies and enhanced oxygen mobility. These changes resulted in improved catalytic performance for the oxidation of light alkanes and CO, with consistent reductions in T_{50} values and a notable increase in aging resistance. The enhanced reducibility observed, particularly in Pt-containing systems, suggests a strong impact at the metal/support interface. Overall, this work highlights post-synthesis ion irradiation as an effective tool for activating and stabilizing redox catalysts, providing new opportunities for designing durable materials for environmental and energy applications.

1. Introduction

In recent years, heterogeneous catalysis has played an increasingly pivotal role across a broad spectrum of industrial applications [1–3], particularly in the control and optimization of combustion processes involving organic compounds such as carbon monoxide (CO), methane (CH_4), propylene (C_3H_6), and hexane (C_6H_{14}) [4–6]. These molecules, extensively employed as fuels or formed as by-products in the energy, chemical, and automotive sectors, are highly reactive. However, their incomplete oxidation can lead to the emission of toxic and environmentally detrimental species, significantly contributing to atmospheric pollution [7,8].

Heterogeneous catalysts facilitate the complete oxidation of these compounds at comparatively low temperatures, enabling their efficient conversion into carbon dioxide (CO_2) and water (H_2O). This not only improves energy efficiency but also minimizes the formation of harmful by-products such as nitrogen oxides (NO_x), residual CO, and unburnt hydrocarbons, offering substantial environmental and technological advantages for cleaner, more sustainable combustion systems [9–11].

Among the most critical applications of this strategy is in automotive exhaust after-treatment, where stringent emission regulations demand efficient and robust catalytic solutions [12–14]. In this context, ceria-based materials have emerged as indispensable components, particularly in three-way catalysts (TWCs) widely used in the automotive industry [15,16].

Their exceptional oxygen storage and release capacity (OSC) [17]

* Corresponding author. Present address: University of Brescia, Via Branze 38, Brescia 25123, Italy.
E-mail address: nancy.artioli@unibs.it (N. Artioli).

https://doi.org/10.1016/j.apcata.2025.120536
Received 1 July 2025; Received in revised form 22 August 2025; Accepted 30 August 2025
Available online 31 August 2025

enables them to dynamically modulate the redox environment, thereby enhancing overall catalyst performance.

When employed as oxide supports, ceria also significantly enhances the catalytic behavior of systems based on transition and rare earth metals [18]. This enhancement is observed across a variety of key reactions, including the water–gas shift reaction [19,20], partial oxidation of methane [21–23], and preferential CO oxidation (PROX) [24,25]. The unique ability of ceria to undergo reversible Ce^{4+}/Ce^{3+} redox cycling, leading to the formation of oxygen vacancies (O_v), lattice distortion, and localized charge compensation—often accompanied by polaron formation [26]—is central to this behavior.

These oxygen vacancies and the resulting structural changes critically influence the catalyst's surface reactivity by altering adsorption, activation, and transformation pathways for reactant molecules. As such, precise control over the chemical composition, defect structure, and morphology of catalytic materials is essential for the rational design of next-generation heterogeneous catalysts with improved activity and selectivity.

Within this framework, interface engineering has emerged as a powerful approach for tailoring catalytic properties at the atomic scale. Among the techniques available, ion beam processing stands out for its versatility and precision in modifying surface and interface characteristics [27]. This method encompasses a variety of mechanisms—including ion implantation, beam mixing, sputtering, and ion–solid interactions [27–29]—that can be finely tuned to manipulate both surface and sub-surface regions of catalytic materials.

Ion beam techniques have enabled the controlled deposition of thin films, incorporation of trace elements, and functionalization of surfaces, as well as the fabrication of mixed-phase interfaces and nano-architectured layers with tailored chemical reactivity [30–34]. In the context of catalysis, ion beam processing has gained increasing attention for the deposition of active metals and dopants on solid supports. For example, Fu et al. [35] used magnetron sputtering to deposit Pt on carbon supports for Proton Exchange Membrane Fuel Cells (PEMFCs), achieving enhanced specific power output compared to commercial catalysts. Similarly, Zlobin et al. [36] applied ion beam sputtering to develop diesel oxidation catalysts with improved activity.

Despite these promising results, ion beam sputtering has primarily been limited to the deposition phase and does not inherently induce structural defects—such as oxygen vacancies—that are known to play a vital role in enhancing catalytic activity in oxide-based systems.

To address this, direct ion irradiation of catalytic supports with light or heavy ions (e.g., He^+, Ar^+, O^+) has emerged as a promising strategy for engineering defect chemistry at the atomic level. This approach enables the generation of controlled surface and bulk defects that can modulate redox behavior, enhance adsorption properties, and ultimately boost catalytic performance. For instance, Kimata et al. [37] demonstrated that ion irradiation as a pre-treatment for carbon supports in PEMFCs led to favorable modifications in both morphology and electrochemical behavior.

However, the practical application of this method poses several challenges. The most critical is the thermal instability of irradiation-induced defects: high-temperature treatments commonly used in catalyst preparation—such as reduction or calcination—can result in partial or complete defect annihilation. Additionally, the impact of such defects on metal nucleation and particle growth is not always predictable, and their influence on final catalytic performance remains highly system-specific. Chemical compatibility between the defect-rich support and the synthesis environment is also a potential concern, as undesired interactions may hinder optimal catalyst functionality.

To circumvent these limitations, in the present study, we explored the application of ion irradiation as a post-synthesis strategy to directly modify the surface properties of a noble metal-supported catalyst, namely Pt (0.5 wt%) supported on $Ce_{0.68}Zr_{0.32}O_2$. Unlike pre-synthesis irradiation, which may suffer from defect instability and incompatibility with subsequent synthesis conditions, the post-synthesis approach allows direct tuning of the active material under controlled conditions, minimizing the risk of defect healing or interference with catalyst preparation protocols.

To evaluate the impact of ion-induced modifications on catalytic performance, we selected a set of representative oxidation reactions involving carbon monoxide (CO), methane (CH_4), propylene (C_3H_6), and hexane (C_6H_{14}). These molecules were chosen as model pollutants and fuel components due to their relevance in emission control from combustion engines and industrial processes, as outlined in the first part of this introduction. The catalytic tests were carried out in the presence of 2000 ppm of each compound in 10 % O_2, simulating conditions typical of lean-burn or exhaust gas environments.

This approach enables a systematic investigation of how post-synthetic ion irradiation affects both the redox behavior of the $Ce_{0.68}Zr_{0.32}O_2$ support and the overall activity of the Pt-based catalyst toward complete oxidation. The results aim to provide mechanistic insights into defect-mediated catalytic processes and offer a pathway for the rational post-treatment engineering of high-performance catalysts for environmental applications.

2. Materials and methods

The ceria-zirconia mixed oxide, $Ce_{0.68}Zr_{0.32}O_2$, (Ce/Zr molar ratio 68/32) was provided by Rhodia (now Solvay). Details on their textural and structural characterization are given in reference [38]. This oxide was impregnated by incipient wetness technique with a $[Pt(NH_3)_4](OH)_2$ solution in order to obtain well dispersed catalyst containing ~0.5 wt% Pt. After drying at 383 K, the catalyst was heated 5 h at 723 K in a dry air flow (heating and cooling rates of 5 K min^{-1}). The Pt content of the Pt/CZ-catalysts has been verified by elemental analysis that estimated a value of 0.58 % w/w. The ionic bombardment modifications of the $Ce_{0.68}Zr_{0.32}O_2$ and $Pt/Ce_{0.68}Zr_{0.32}O_2$ samples were achieved by a micro-accelerator using a N^+ ion beam working at 52.5 keV with nitrogen partial pressure of 10^{-5} mbar, which gives a current density of 3.75 μA/cm^2. The incident angle of N ions was 0° from surface normal.

CO chemisorption measurements were carried out at 313 K using a pulsed CO uptake method on a Micromeritics ASAP 2020 instrument. Before analysis, samples were reduced under 10 % H_2/Ar at 623 K for 1 h and then cooled under He. Dispersion values were calculated assuming a 1:1 CO/Pt adsorption stoichiometry, and are expressed as the percentage of surface-exposed Pt atoms relative to the total Pt content.

Temperature-programmed oxidation (TPO) and Temperature programmed reduction (TPR) experiments have been performed in an IR reactor cell. The catalyst (20–25 mg), in the form of a self-supporting wafer, was situated in the infrared cell. A thermocouple allowed following the exact temperature of the catalyst. Gas was introduced into the system by mass flow controllers (Brooks 5850E) and mixed in a single stream before entering the reactor, whereas the exit stream was simultaneously analyzed by quadrupole mass spectrometer (Balzers Omnistar GSD 300 O) and FTIR spectrometer (via a gas microcell of 0.088 cm^3 volume). IR spectra were collected with a Thermo Scientific Nicolet 6700 FTIR spectrometer, equipped with MCT detectors, and accumulating 64 scans at a resolution of 4 cm^{-1}. More details can be found in the following references for both the IR *operando* system and the IR reactor-cell [39,40]. TPO tests were carried out by flowing 2000 ppm of CO, CH_4, C_3H_6 and C_6H_{14} and 10 % O_2 in Ar (GHSV 50–60 $m^3\,kg^{-1}\,h^{-1}$) for 90 min at room temperature, and then the temperature was gradually increased from 20 to 823 K at 2 K min^{-1}. In order to feed a fixed concentration of vaporized hexane, the system was implemented by a saturator located in a thermostatic bath. Three consecutive TPO cycles were performed in order to reach stationary working conditions of the catalysts. The light-off temperatures obtained in the third catalytic cycle are reported in the paper. TPR tests were performed implying H_2 as a reductant (4000 ppm in argon, flow 25 Ncc/min) and increasing the temperature from ambient temperature to 823 K at 5 K/min, holding for 90 min. The catalyst then was cooled down to 293 K in hydrogen

5 K/min. For the FTIR study of the H_2 reduction, samples were (i) exposed to 13 kPa of H_2 at room temperature then (ii) heated for 0.5 h at the temperature of reduction (Tr), (iii) quenched under H_2 at ambient temperature to record the spectrum, and (iv) evacuated and heated to Tr for 0.25 h under vacuum before being quenched at ambient temperature for spectrum recording. This sequence (i-iv) was repeated 3 times. The cycles were repeated for Tr varying from 373 to 873 K. Electron microscopy was carried using a Tecnai G2 30 UT operating at 300 kV acceleration voltage with a 0.17 nm point resolution. The images were recorded from a 3-mm diameter specimen mounted on a double tilt holder in a conventional CompuStage that enables a tilting range of $\pm 20–29^0$. For the TEM analysis, the sample has been crushed in ethanol and a drop of the mixture has been placed on the TEM grid for analysis.

XPS (X-ray Photoelectron Spectroscopy) surface chemical analyses were carried out with a Thermo Electron K-Alpha spectrometer using a monochromatic Al-Kα X-Ray source (1486.6 eV). The Thermo Electron K-Alpha spectrometer procedure was used to calibrate the spectrometer. It was verified using Cu and Au (Au 4f7/2 at 84.0 eV) samples following the ASTM-E-902–94 standard procedure. Acquisition parameters implied in this study were the following: 400 μm spot size, 12 kV primary energy, 6.0 mA emission intensity, CAE 50 eV and 0.1 eV energy step size. Quantification was performed with the Thermo Fisher scientific Avantage© data system. As mentioned in the text, strong local charge effect was observed on powders after bombardment. For this reason, an antistatic gun (*Milty Zerostat 3 anti-static Gun)* has been used and the analyses have been performed in floating mode (sample completely isolated from the stage).

3. Result and discussion

The effect of ion irradiation on the catalytic behavior of $Ce_{0.68}Zr_{0.32}O_2$-based materials was first evaluated through temperature-programmed oxidation (TPO) experiments, using CO, CH_4, C_3H_6, and C_6H_{14} as representative oxidation targets. These molecules were selected due to their relevance in emission control and fuel combustion applications, where incomplete oxidation leads to the release of harmful pollutants [16,25,41]. Each reactant was introduced at 2000 ppm in a 10 % O_2/Ar mixture, and the temperature was ramped from ambient to 823 K.

Fig. 1A and B report the conversion profiles for the bare $Ce_{0.68}Zr_{0.32}O_2$ and the Pt-supported counterpart, respectively, before and after ion irradiation. In all cases, the irradiated catalysts (solid symbols) exhibit enhanced conversion at lower temperatures compared to the untreated samples (hollow symbols), demonstrating improved oxidation kinetics across the tested temperature range. To quantify this enhancement, Table 1 lists the T_{50} values (temperature at which 50 % conversion is achieved) for each reactant. In the case of the bare support, T_{50} for CO, C_3H_6, and C_6H_{14} decreased by 10–20 K upon irradiation. This effect is even more pronounced in the Pt-containing catalyst, where T_{50} reductions reached 40–60 K. For instance, CO conversion improved from 640 K to 579 K after treatment. These shifts are particularly significant for Ce–Zr materials, whose redox properties are sensitive to the presence of oxygen vacancies and defect sites that facilitate oxygen mobility and molecular activation [17,42]. While methane showed limited conversion in all cases, as expected due to its high C–H bond dissociation energy, a slight increase in CH_4 reactivity was observed for the $Pt/Ce_{0.68}Zr_{0.32}O_2$ catalyst after bombardment (from 8.4 % to 9.4 % at 823 K). This subtle change supports the idea that even weakly reactive species may benefit from the defect-rich surface and improved oxygen activation capacity induced by ion treatment. It is important to note that $Pt/Ce_{0.68}Zr_{0.32}O_2$ already outperforms the bare oxide due to the dual contribution of noble metal sites and the Ce-based redox support [18,24,43]. The additional enhancement observed after irradiation suggests that the treatment not only increases the surface reactivity of the support but also modifies the metal–support interface in a way that promotes more efficient oxidation. This is in line with studies showing that oxygen mobility, Ce^{3+} surface enrichment, and metal dispersion play synergistic roles in boosting catalytic performance [44,45]. These results clearly demonstrate that post-synthesis ion irradiation leads to a general improvement in catalytic performance for oxidation reactions, and provide the first indication of structural and electronic changes that will be further explored in the subsequent paragraphs.

Table 1
T_{50} values of representative pollutants Temperature-programmed oxidation (TPO) measurements. The table reports the temperature that corresponds to the achievement of 50 % of conversion for CO, C_3H_6, C_6H_{14} measured on $Ce_{0.68}Zr_{0.32}O_2$ and $Pt/Ce_{0.68}Zr_{0.32}O_2$ catalysts both before and after ionic bombardment. Since the conversion of the CH_4, in these experiments is low (less than 10 %) in all cases, in the table is reported the value of the conversion achieved at maximum temperature (823 K).

	$Ce_{0.68}Zr_{0.32}O_2$		$Pt/Ce_{0.68}Zr_{0.32}O_2$	
	non treated	bombarded	non treated	bombarded
T_{50} CO (K)	739	696	640	579
T_{50} C_3H_6 (K)	756	738	682	645
T_{50} C_6H_{14} (K)	764	754	693	660
Conversion % CH_4 at 823 K	4.2	4.9	8.4	9.4

The redox properties of the catalysts were examined by H_2-temperature programmed reduction (H_2-TPR) to assess the impact of ion irradiation on hydrogen uptake and reducibility. Experiments were conducted on both $Ce_{0.68}Zr_{0.32}O_2$ and $Pt/Ce_{0.68}Zr_{0.32}O_2$ samples, before and after nitrogen ion bombardment, under a 4000 ppm H_2/Ar mixture

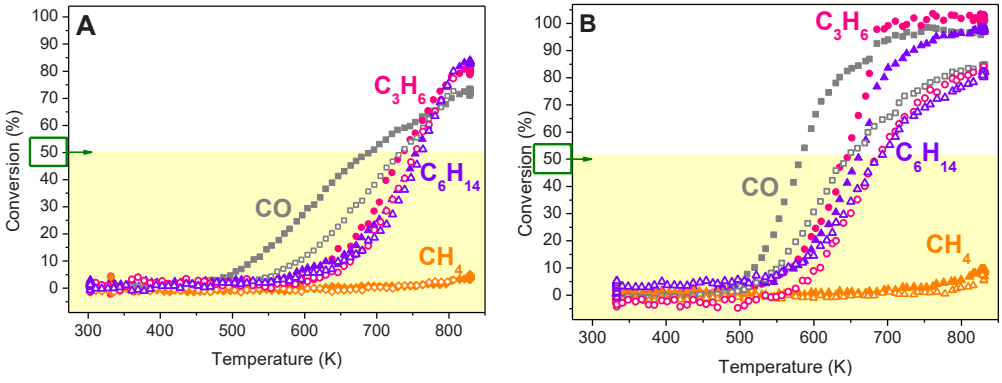

Fig. 1. Representative pollutants Temperature-programmed oxidation (TPO) measurements. The conversion of the different species measured in the catalytic tests is reported versus the temperature for $Ce_{0.68}Zr_{0.32}O_2$ (Fig. 1A) and Pt/ $Ce_{0.68}Zr_{0.32}O_2$ (Fig. 1B) catalysts. In particular, for each catalytic system is reported the conversion before (empty symbols) and after (full symbols) the ion bombardment for CO (□,■), CH_4 (◇,□), C_3H_6 (○,●,) and C_6H_{14} (△,▲).

with a ramp rate of 5 K min^{-1}. Fig. 2A displays the TPR profile for the bare $Ce_{0.68}Zr_{0.32}O_2$. The untreated sample exhibits a broad reduction peak centered at approximately 685 K, which corresponds to the progressive reduction of Ce^{4+} to Ce^{3+} in the bulk and sub-surface layers, consistent with literature data for Ce–Zr mixed oxides [42]. After ion irradiation, the reduction peak shifts substantially to lower temperature (~585 K), indicating an increased reducibility of the catalyst. This behavior is typically associated with the formation of oxygen vacancies and an increased presence of labile oxygen species. Nonetheless, the observed redox enhancement is consistent with defect formation mechanisms that are known to facilitate oxygen exchange processes in ceria-based systems [46]. In the case of the Pt-containing catalyst (Fig. 2C), the introduction of noble metal significantly alters the reduction behavior. The untreated $Pt/Ce_{0.68}Zr_{0.32}O_2$ sample exhibits a sharp and well-defined reduction peak centered at 521 K, which is attributed to hydrogen spillover from Pt sites to the reducible ceria–zirconia support [45]. Following ion bombardment, the main peak undergoes a remarkable downshift to 340 K, indicating a drastic improvement in low-temperature reducibility. This shift reflects the combined effects of surface and sub-surface defect formation, and enhanced hydrogen spillover from Pt to the support [47]. It is important to note that the magnitude of the temperature shift is greater in the Pt-loaded system (~180 K) than in the bare support (~100 K), highlighting a synergistic enhancement of reducibility due to the concurrent effects of Pt dispersion and irradiation-induced disorder.

The observed improvement in reducibility is consistent with literature reported by Clark et al. [47], which demonstrated that Pd nanoparticles can significantly promote ceria reduction through hydrogen spillover mechanisms, even at low temperatures. Their study showed that Ce(IV) is reduced to Ce(III) below 150 °C in the presence of Pd, and that surface oxygen vacancies act as favorable sites for hydrogen adsorption and migration. Hence, rather than hindering Ce reduction, the vacancy-rich surface facilitates hydrogen spillover and redox activation, consistent with the downshift observed in the TPR profiles. The ion beam treatment additionally modifies the electronic environment at the metal–support interface, further promoting low-temperature reduction.

These TPR observations correlate well with TPO results. The increased availability of labile lattice oxygen and the decreased energy required for Ce^{4+} reduction are key factors contributing to the observed

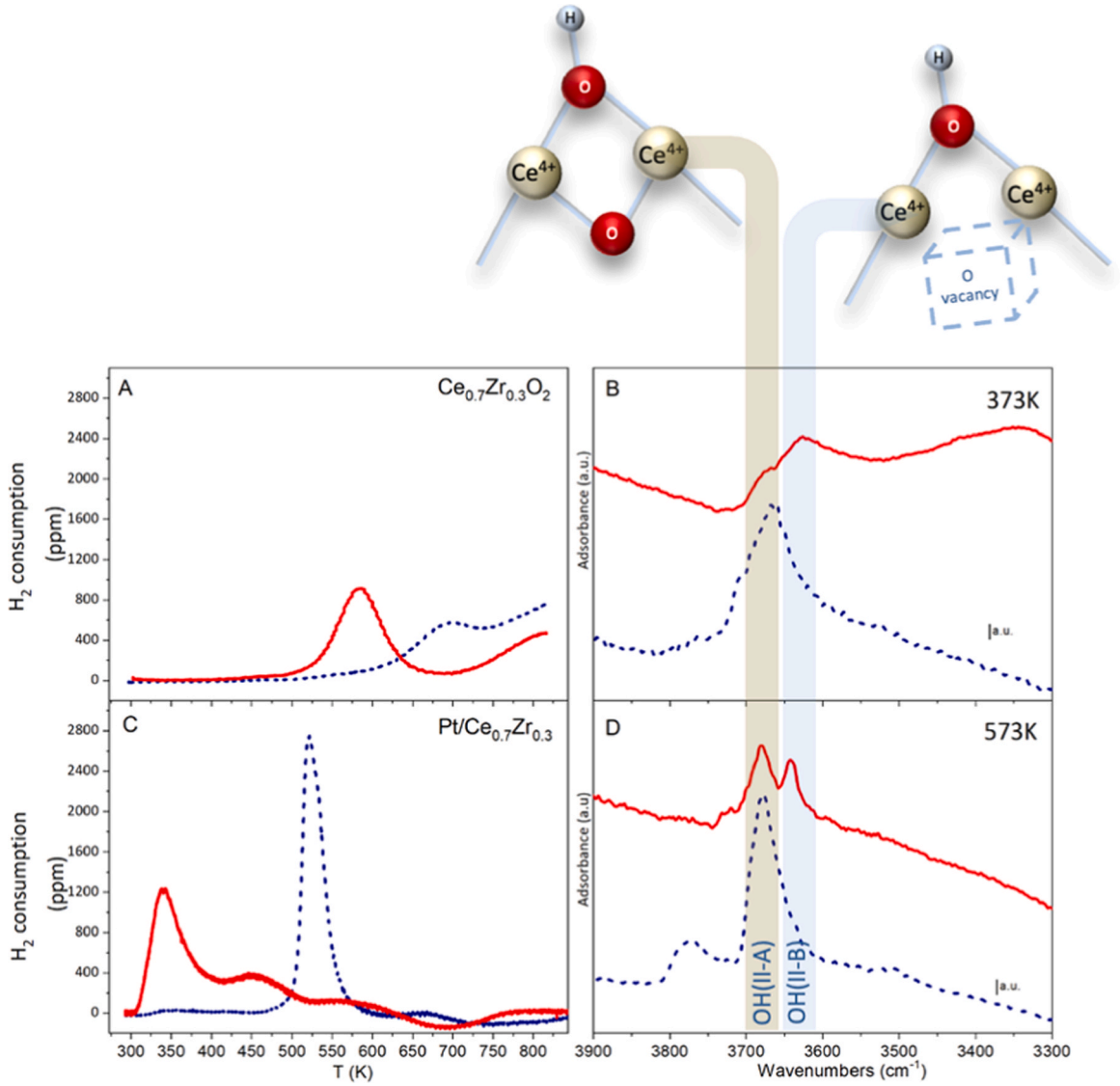

Fig. 2. Temperature programmed reduction (TPR) experiments. It reports on the left side the H_2 consumption versus the temperature measured on TPR experiments on $Ce_{0.68}Zr_{0.32}O_2$ (A) and $Pt/Ce_{0.68}Zr_{0.32}O_2$ (C) catalysts before (blue) and after (red) ionic bombardment. On the right are reported the spectra of $Ce_{0.68}Zr_{0.32}O_2$ (B) and $Pt/Ce_{0.68}Zr_{0.32}O_2$ (D) sample in the νOH region before (blue) and after (red) ionic bombardment after 3 × 0.5 h of 13kPa H_2 treatment at different temperatures (373 K (B) and 573 K (D)).

decrease in light-off temperatures for CO and hydrocarbon oxidation. These results confirm that nitrogen ion irradiation is a powerful post-synthesis tool for activating redox functionality in ceria-based systems. By lowering the temperature threshold for hydrogen uptake, it promotes the creation of reactive oxygen species at the catalyst surface, ultimately improving catalytic efficiency and expanding the operating window for oxidation processes.

To further investigate the surface modifications induced by ion irradiation, operando FTIR studies were carried out to monitor the evolution of hydroxyl groups during H_2 reduction. The vibrational features in the ν(OH) region were used as probes to assess the surface oxidation state and the presence of specific adsorbed species associated with cerium coordination and defect structures. Figs. 2B and 2D report the FTIR spectra of $Ce_{0.68}Zr_{0.32}O_2$ and $Pt/Ce_{0.68}Zr_{0.32}O_2$, respectively, before and after ion irradiation, following exposure to 13 kPa of H_2 at different reduction temperatures. The spectra were recorded after each of three consecutive H_2 treatments, separated by evacuation steps and performed in the range 373–573 K.

In the case of $Ce_{0.68}Zr_{0.32}O_2$ (Fig. 2B), spectra acquired after reduction at 573 K display distinct bands in the 3600–3700 cm^{-1} region, which correspond to different types of hydroxyl groups bound to the oxide surface. The two main features, labeled II-A and II-B following the classification of Daturi et al. [45], are attributed to bridged hydroxyl species (Ce–OH–Ce) and terminal hydroxyls located near oxygen vacancies (Ce–OH·V_o), respectively. Upon ion irradiation, the intensity of the II-B band increases significantly relative to the II-A band, suggesting an increased density of coordinatively unsaturated Ce sites and a higher concentration of surface oxygen vacancies. This observation is consistent with the improved reducibility revealed by TPR data. The effect is even more pronounced in the Pt-containing catalyst (Fig. 2D). After irradiation, the II-B hydroxyl band appears already at 373 K, a temperature ~200 K lower than the one at which the same feature becomes detectable in the bombarded support alone. This shift provides strong evidence of a synergistic effect between Pt and the defect-rich Ce–Zr oxide support: the presence of Pt not only facilitates hydrogen dissociation via spillover but also promotes the stabilization of reactive hydroxyl species at lower temperatures. Such behavior is indicative of a strengthened metal–support interaction and the presence of highly labile surface oxygen species. Overall, the FTIR results corroborate the TPR findings and confirm that ion irradiation enhances the redox flexibility of both the support and the metal–support interface. The increased intensity and evolution of these hydroxyl bands provide further insight into the modified surface reactivity induced by ion bombardment. The increased population of surface hydroxyl groups is consistent with a higher concentration of labile oxygen species and defect sites, such as oxygen vacancies [46].

High-resolution transmission electron microscopy (HRTEM) was employed to investigate the microstructural effects induced by nitrogen ion irradiation on the $Pt/Ce_{0.68}Zr_{0.32}O_2$ catalyst. Representative images of the catalyst before and after bombardment are shown in Fig. 3A/A'

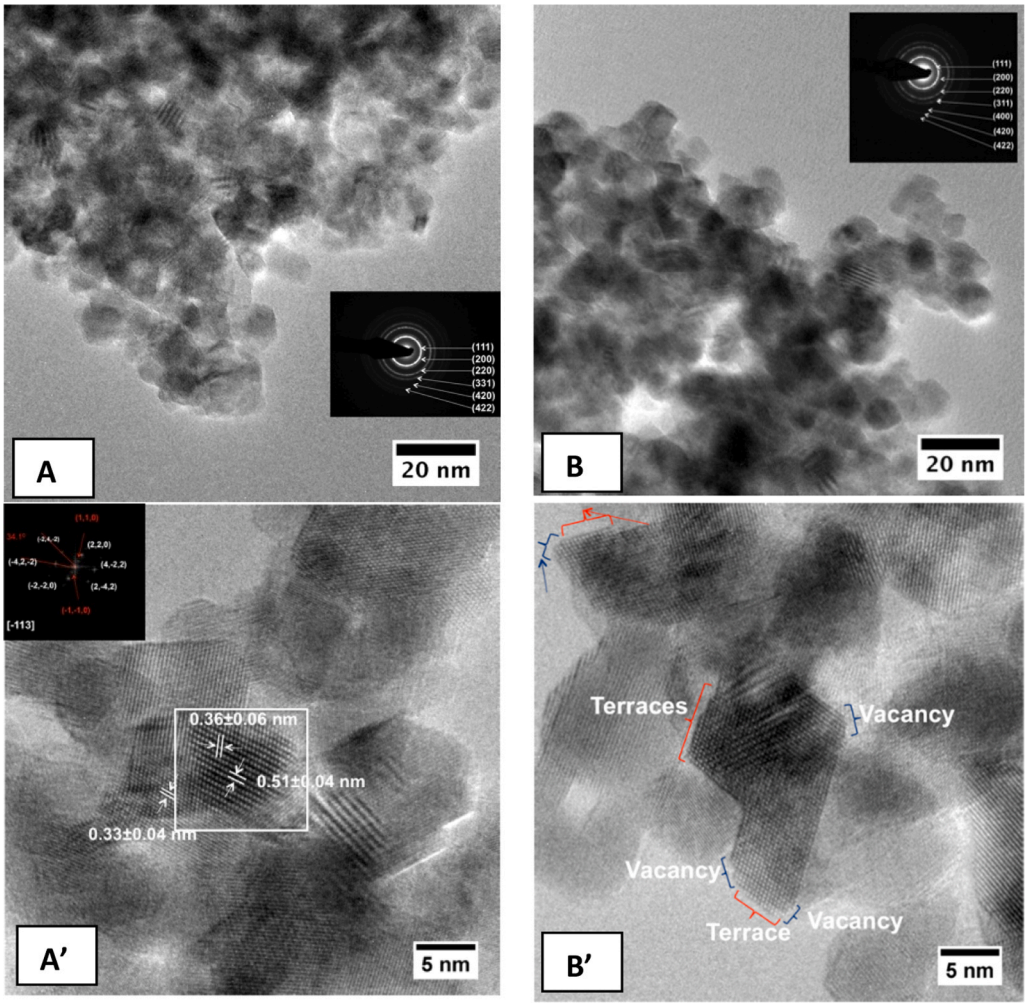

Fig. 3. Low magnification TEM images of the sample containing Platinum (Pt) nanoparticles supported on $Ce_{0.68}Zr_{0.32}O_2$ substrate: **(A)** before ion bombardment and **(B)** after ion bombardment, both with in the inset a SAED pattern indexed considering the structure of $Ce_{0.68}Zr_{0.32}O_2$. High Resolution TEM (HRTEM) images of the same sample: **(A′)** before ion bombardment, with in the inset the corresponding FFT pattern, and **(B′)** after ion bombardment.

and 3B/B', respectively. The untreated sample (Figs. 3A and 3A') displays well-defined, highly faceted nanoparticles with crystalline domains, indicative of a well-ordered fluorite structure typical of Ce–Zr oxides. Notably, the presence of superlattice features was observed in several particles, as evidenced by additional reflections in the Fast Fourier Transform (FFT) pattern (inset of Fig. 3A'). These reflections, which appear in forbidden positions for the ideal fluorite structure, are consistent with cation ordering phenomena, possibly due to local Zr segregation or vacancy ordering, as previously reported [48]. After ion irradiation (Figs. 3B and 3B'), significant morphological changes are apparent. The overall crystallinity of the particles is reduced, with visible signs of surface amorphization, increased defect density, and the emergence of atomic-scale terraces and vacancies at the nanoparticle edges. These features are highlighted in the micrograph by arrows and braces. Indeed, it is well established in the literature that during the formation of oxygen vacancies, the outermost oxygen atoms are initially removed, creating vacancies, while the sub-surface oxygen atoms progressively migrate to the surface to occupy these sites. As the vacancy concentration increases, they gradually diffuse into the bulk. This process is accompanied by distortions of the cerium lattice, which facilitate the rapid migration of oxygen vacancies [49]. Such lattice distortions are also visible in the TEM images and provide indirect evidence of oxygen vacancy formation, fully consistent with previous reports [50]. Consequently, the loss of long-range periodicity and the emergence of disordered domains indicate that the ion beam has introduced extended structural defects, disrupting the previously ordered cation lattice [28, 51]. The enhanced surface disorder and formation of low-coordination sites are expected to contribute positively to catalytic performance. These features are commonly associated with higher oxygen vacancy concentration and increased reactivity due to the presence of coordinatively unsaturated surface atoms [5,8]. Additionally, ion bombardment appears to promote the formation of secondary phases. Selected area electron diffraction (SAED) patterns and HRTEM contrast suggest the emergence of minor monoclinic ZrO_2 domains, coexisting with the predominant cubic $Ce_{0.68}Zr_{0.32}O_2$ phase (Fig. 3B). This phase segregation is likely driven by local heating and energy dissipation during ion impacts, which may induce partial crystallographic reconstruction. Furthermore, the Pt nanoparticles are more finely dispersed after irradiation, with no evidence of extensive sintering. This behavior is consistent with the hypothesis that ion bombardment promotes partial embedding or anchoring of metal particles into the oxide surface due to localized melting or softening phenomena at the interface [34,51]. Such anchoring can enhance metal–support adhesion and improve thermal stability—an effect supported by complementary FTIR chemisorption data on aged catalysts.

The excellent dispersion and thermal stability of Pt particles in the irradiated sample suggest a stronger interaction with the support, potentially related to partial embedding or anchoring effects induced by the ion beam treatment. While our TEM analysis does not allow direct observation of embedding, such behavior is supported by prior studies showing that ion irradiation can introduce oxygen vacancies, surface defects, and interfacial restructuring that strengthen metal–support interactions. For example, Wang et al. [32] reported that Ar^+ bombardment of CeO_2 leads to the formation of anchoring sites through preferential oxygen removal, while Cairns et al. [52] and Kimata et al. [37] observed enhanced adhesion and stability of Pt nanoparticles due to ion-induced interface engineering. The improved resistance to sintering observed in our study is consistent with these mechanisms, although further high-resolution structural characterization would be necessary to confirm nanoparticle embedding.

Altogether, the HRTEM analysis provides direct visual confirmation of the irradiation-induced modifications at the nanoscale, revealing a complex interplay of amorphization, surface restructuring, and local phase transformation. These microstructural changes are intimately linked to the enhanced redox behavior and catalytic activity observed.

To investigate the electronic and chemical modifications induced by ion irradiation, X-ray photoelectron spectroscopy (XPS) analyses were conducted on $Pt/Ce_{0.68}Zr_{0.32}O_2$ catalysts, comparing untreated and irradiated samples. Particular focus was placed on the Pt 4 f and O 1 s core-level regions (Figs. 4A and 4B). In the fresh, non-irradiated catalyst, the Pt 4 $f_{7/2}$ peak was centered around 71.2 eV, indicative of metallic platinum in a highly dispersed state, consistent with previous studies on Pt/ceria–zirconia systems [45]. The O 1 s region exhibited a dominant contribution at ~529.2 eV, assigned to lattice oxygen, with a minor component at higher binding energy (~531.5 eV) related to surface hydroxyls and oxygen species in non-stoichiometric or defective environments. Following ion irradiation, In the Pt 4 f region (Fig. 4A), the relative intensity of the metallic Pt signal decreased, yet without a corresponding increase in the oxidized species. After thermal aging, both treated and untreated samples showed a further decline in Pt^0 intensity. These trends suggest a loss in metallic Pt accessibility, potentially due to partial embedding or coverage by the support, rather than a true increase in oxidation state. This interpretation is consistent with the findings of Wang et al.[53], who demonstrated that stronger Pt–CeO_2 interactions induced by thermal treatment may not lead to a detectable oxidation of Pt, as the metal remains largely in the metallic state despite enhanced interfacial bonding. The Ce 3d spectra confirmed an increase in Ce^{3+} content in the irradiated sample, in line with oxygen vacancy formation. Therefore, the observed XPS changes can be attributed to structural rearrangements and defect-mediated anchoring rather than electronic oxidation of Pt, likely driven by local surface heating and sub-surface mixing during ion impacts [34,51]. These observations are consistent with enhanced Pt anchoring or partial encapsulation by the oxide matrix, a behavior previously reported in ion-treated catalysts [28,31].

In the O 1 s region (Fig. 4B), the high-binding-energy component increased in intensity after irradiation, pointing to a higher concentration of defective oxygen species and surface hydroxyls. This is in excellent agreement with the higher oxygen mobility and vacancy density inferred from TPR and FTIR results. The chemical shift also reflects the presence of under-coordinated oxygen atoms at irradiation-induced defect sites, which are known to act as active centers for oxidation reactions[34,45]. Furthermore, the irradiated samples displayed severe localized charging during XPS analysis, requiring the use of floating mode and antistatic neutralization. This behavior is indicative of heterogeneous surface conductivity and spatial charge accumulation at defective or insulating domains, typical of ion-bombarded oxide materials [34,51]. Although the overall elemental composition remained nearly unchanged post-treatment, the XPS data reveal significant modifications in the local electronic structure. These include the generation of oxygen vacancy-related species, increased surface hydroxylation, and altered Pt electronic environments—all of which are strongly correlated with the enhanced reducibility and improved oxidation performance observed in catalytic testing. In summary, XPS analysis confirms that nitrogen ion irradiation modifies both the oxide support and the supported metal phase at the electronic level. The generation of electronically distinct oxygen environments and the redistribution of Pt species contribute directly to the improved redox activity and catalytic stability of the materia

Beyond enhancing redox properties and surface reactivity, ion irradiation also exerts a beneficial effect on the long-term thermal stability of catalytic material. To evaluate this, additional tests were performed on commercial benchmark oxidation catalysts consisting of 1 wt% Pt/Al_2O_3, 1 wt% Pd/Al_2O_3, and bimetallic 0.5 wt% Pt–0.5 wt% Pd/Al_2O_3, commonly used in automotive emission control. These systems served as model substrates to assess whether the irradiation strategy could be generalized to noble-metal catalysts supported on non-redox, thermally insulating oxides.

CO adsorption followed by FTIR spectroscopy was used to probe Pt dispersion on the commercial Pt/Al_2O_3 catalyst before and after nitrogen ion irradiation, and again after thermal aging. The untreated catalyst exhibited an initial metal dispersion of ~38 %, which remained nearly

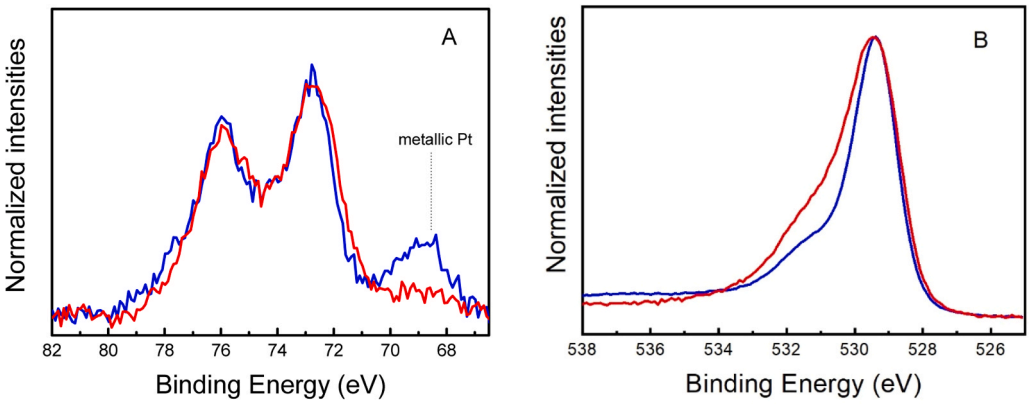

Fig. 4. XPS spectra of $Ce_{0.68}Zr_{0.32}O_2$:Pt before (blue)and after (red) ion bombardment in the Pt4f (a) and O1s region (b).

unchanged after irradiation, confirming that the ion beam treatment does not compromise the accessibility of active Pt sites under fresh conditions. However, following accelerated thermal aging, the dispersion dropped significantly to 15 % in the untreated sample, whereas it remained at 26 % in the irradiated sample. This notable difference highlights the role of ion bombardment in enhancing the thermal stability of Pt nanoparticles and mitigating sintering phenomena. Ion irradiation is known to introduce defect structures and anchor sites on oxide supports, which can act as nucleation centers or physical barriers, limiting metal atom migration and coalescence during high-temperature treatments. As reported by Magudapathy et al. [54], ion-induced surface modifications can enhance the interaction between metal nanoparticles and the support, improving their dispersion and resistance to sintering. In our case, the retention of higher Pt dispersion after aging suggests that the defects and structural rearrangements induced by irradiation create a more robust anchoring environment, capable of suppressing particle growth and deactivation under harsh conditions.

The stabilizing effect is likely attributable to local surface melting and re-solidification triggered by ion impacts, which may induce partial embedding of metal particles into the support, thereby improving their anchorage [34,51]. This phenomenon was previously observed in ion-treated oxide-supported systems and is consistent with the morphological changes identified via HRTEM.

In parallel, catalytic activity and stability tests were conducted on Pt/Al_2O_3, Pd/Al_2O_3, and $Pt–Pd/Al_2O_3$ formulations. The results, summarized in Table 2, were obtained under the same reaction conditions, enabling direct comparison with the Pt/CZ system. Upon irradiation, the T_{50} values for propene and hexane oxidation decreased from 490 K to 466 K and from 683 K to 653 K, respectively. These improvements suggest better oxygen activation and transport, even in the absence of a redox-active support, and confirm that the structural integrity of active sites is retained.

However, the overall impact of ion irradiation on alumina-supported catalysts was limited. This is likely due to the inert nature of Al_2O_3, which lacks the redox flexibility and defect chemistry of ceria-based supports. Among the Al_2O_3-supported materials, the Pt–Pd formulation showed the best response to irradiation, but its thermal stability remained lower than that of the irradiated Pt/CZ system. In contrast, ion treatment of Pt/CZ led to a pronounced enhancement in both activity retention and redox behavior. When benchmarked against literature-reported ceria–zirconia-supported Pt catalysts (Table 1), the irradiated Pt/CZ sample demonstrates comparable or superior thermal durability. These results highlight that the beneficial effects of ion bombardment are most effective when applied to redox-active supports like $Ce_{0.7}Zr_{0.3}O_2$, where defect formation, oxygen storage, and strong metal–support interactions work synergistically to improve performance.

Importantly, this approach also offers value for industrially relevant catalysts supported on non-reducible oxides. While the enhancements are less pronounced, ion beam treatment still contributes to improved thermal stability, widening the applicability of this method as a scalable post-synthesis strategy to preserve metal dispersion and catalytic performance under harsh oxidative conditions.

4. Conclusions

This study demonstrates the significant potential of post-synthesis ion beam irradiation as a surface engineering strategy to enhance the performance and stability of ceria–zirconia-based oxidation catalysts. Nitrogen ion bombardment was shown to induce both structural and electronic modifications in $Ce_{0.68}Zr_{0.32}O_2$ supports, with and without platinum, leading to improvements in reducibility, oxygen mobility, and overall catalytic activity. A key outcome of this work is the correlation between ion-induced defect formation—particularly oxygen vacancies—and enhanced redox behavior, as evidenced by lower T_{50} values in

Table 2
T_{50} values of representative pollutants Temperature-programmed oxidation (TPO) measurements. The table reports the temperature that corresponds to the achievement of 50 % of conversion for CO, C_3H_6, C_6H_{14} measured on 1 % Pd/Al_2O_3 and $Pt–Pd/Al_2O_3$ catalysts before and after ionic bombardment, and before and after ageing along with the conversion of the CH_4 achieved at maximum temperature (823 K.1.

NOT AGED	**1 %Pt/ϒAl_2O_3**		**1 %Pd/ϒAl_2O_3**		**0.5 %Pt-0.5 Pd/ϒAl_2O_3**	
	non treated	bombarded	non treated	bombarded	non treated	bombarded
T_{50} CO (K)	448	445	465	455	457	450
T_{50} C_3H_6 (K)	490	466	501	482	459	443
T_{50} C_6H_{14} (K)	683	653	652	602	541	506
Conversion % CH_4 at 823 K	14 %	16 %	82 %	85	42	43
AGED	**1 %Pt/ϒAl_2O_3**		**1 %Pd/ϒAl_2O_3**			
	non treated	bombarded	non treated	bombarded		
T_{50} CO (K)	450	451	450	452		
T_{50} C_3H_6 (K)	464	458	467	460		
T_{50} C_6H_{14} (K)	467	461	595	581		
Conversion % CH_4 at 823 K	29	29	92	94		

oxidation reactions and earlier onset of OH-related vibrational features in operando FTIR studies. These effects are especially pronounced in Pt-containing catalysts, where irradiation appears to improve metal dispersion and strengthen metal–support interactions. This enhanced interface contributes to better reducibility at low temperature and improved resistance to sintering during aging, as supported by chemisorption and microscopy data.

High-resolution TEM revealed a post-irradiation restructuring of the catalyst surface, with increased occurrence of surface terraces, atomic vacancies, and disordered regions, consistent with enhanced catalytic reactivity. XPS analysis further confirmed localized changes in chemical states, especially in the oxygen and platinum environments, with evidence of partial charge redistribution and altered electronic structure. Moreover, the beneficial effects of ion bombardment were not limited to Ce–Zr-based systems. Additional experiments on commercial

Pt/Al_2O_3 and Pd/Al_2O_3 catalysts confirmed that ion irradiation improves resistance to deactivation and thermal aging, while maintaining or even enhancing oxidation activity. These findings suggest that the advantages of ion beam treatment may be broadly applicable across a range of catalytic materials, not only for redox-active oxides but also for inert supports used in industrial applications. Overall, the results provide compelling evidence that ion beam processing is a viable and scalable post-synthesis method to activate and stabilize heterogeneous catalysts. By creating tailored defect structures and optimizing metal–support interfaces, this technique enables precise tuning of catalyst properties without altering the bulk composition. As such, it represents a valuable tool for the rational design of next-generation catalytic systems targeting environmental remediation and energy conversion technologies.

CRediT authorship contribution statement

Séverine Rousseau: Validation, Resources, Investigation, Funding acquisition, Data curation, Conceptualization. **Arnaud Etcheberry:** Supervision, Investigation, Formal analysis, Data curation. **Denis Busardo:** Visualization, Validation, Resources, Methodology, Data curation. **Philippe Bazin:** Resources, Formal analysis, Conceptualization. **Damien Aureau:** Methodology, Investigation, Data curation. **Hanna Solt:** Visualization, Investigation, Data curation. **Marco Daturi:** Writing – review & editing, Supervision, Resources, Methodology, Investigation, Funding acquisition, Conceptualization. **Marina Maddaloni:** Writing – review & editing, Validation. **Nancy Artioli:** Writing – review & editing, Writing – original draft, Supervision, Project administration, Methodology, Investigation, Formal analysis, Conceptualization. **Alina Bruma:** Writing – original draft, Methodology, Investigation, Formal analysis, Conceptualization. **Sylvie Malo:** Writing – original draft, Software, Investigation, Data curation. **Gilbert Blanchard:** Supervision, Resources, Conceptualization. **Najat Moral:** Visualization, Supervision, Conceptualization.

Associated content

Additional experimental results are supplied as Supporting Information. This material is available free of charge via the Internet at http://pubs.acs.org.

Funding sources

ANR funded project (ID: ANR-10-VPTT-0003).

Declaration of Competing Interest

The authors declare the following financial interests/personal relationships which may be considered as potential competing interests: Nancy Artioli reports financial support was provided by ENSICAEN, Université de Caen. Marco Daturi reports a relationship with French National Research Agency that includes: funding grants ID: ANR-10-VPTT-0003. If there are other authors, they declare that they have no known competing financial interests or personal relationships that could have appeared to influence the work reported in this paper.

Appendix A. Supporting information

Supplementary data associated with this article can be found in the online version at doi:10.1016/j.apcata.2025.120536.

Data Availability

Data will be made available on request.

References

[1] H. Yang, G. Li, G. Jiang, Z. Zhang, Z. Hao, Heterogeneous selective oxidation over supported metal catalysts: from nanoparticles to single atoms, Appl. Catal. B 325 (2023), https://doi.org/10.1016/j.apcatb.2023.122384.
[2] Y. Ren, Y. Yang, M. Wei, Recent advances on heterogeneous non-noble metal catalysts toward selective hydrogenation reactions, ACS Catal. 13 (2023) 8902–8924, https://doi.org/10.1021/acscatal.3c01442.
[3] A. Boontanom, M. Maddaloni, P. Suwanpinij, I. Vassalini, I. Alessandri, Industrial waste against pollution: mill scale-based magnetic hydrogels for rapid abatement of Cr(vi), Environ. Sci. (Camb.) 10 (2024) 551–564, https://doi.org/10.1039/d3ew00490b.
[4] L. Wang, F. Dong, Y. Meng, Y. Kang, H. Zhang, Z. Tang, Molecular sieve confined catalysts for the catalytic combustion of VOCs: preparation, application and future development, J. Mater. Chem. A Mater. (2025), https://doi.org/10.1039/d5ta01092f.
[5] J. Chen, H. Arandiyan, X. Gao, J. Li, Recent advances in catalysts for methane combustion, Catal. Surv. Asia 19 (2015) 140–171, https://doi.org/10.1007/s10563-015-9191-5.
[6] J. Oh, A. Boucly, J.A. van Bokhoven, L. Artiglia, M. Cargnello, Palladium catalysts for methane oxidation: old materials, new challenges, Acc. Chem. Res 57 (2024) 23–36, https://doi.org/10.1021/acs.accounts.3c00454.
[7] M. Maddaloni, A. Centeno-Pedrazo, S. Avanzi, N.J. Mazumdar, H. Manyar, N. Artioli, Novel ionic liquid synthesis of bimetallic Fe–Ru catalysts for the direct hydrogenation of CO2 to short chain hydrocarbons, Catalysts 13 (2023), https://doi.org/10.3390/catal13121499.
[8] M. Maddaloni, M. Marchionni, A. Abbá, M. Mascia, V. Tola, M.P. Carpanese, et al., Exploring the viability of utilizing treated wastewater as a sustainable water resource for Green hydrogen generation using solid oxide electrolysis cells (SOECs), Water (Switzerland) 15 (2023), https://doi.org/10.3390/w15142569.
[9] Y. Pan, N. Li, K. Li, S. Ran, C. Wu, Q. Zhou, et al., Enhanced low-temperature behavior of selective catalytic reduction of NOx by CO on Fe-based catalyst with looping oxygen vacancy, Chem. Eng. J. 461 (2023), https://doi.org/10.1016/j.cej.2023.141814.
[10] L. Lietti, L. Righini, L. Castoldi, N. Artioli, P. Forzatti, Labeled 15NO study on N2 and N2O formation over Pt-Ba/Al2O3 NSR catalysts, Top. Catal. 56 (2013) 7–13, https://doi.org/10.1007/s11244-013-9920-9.
[11] D. La Corte, M. Maddaloni, R. Vahidzadeh, M. Domini, G. Bertanza, S.U. Ansari, et al., Recovered ammonia as a sustainable energy carrier: innovations in recovery, combustion, and fuel cells, Energies (Basel) 18 (2025), https://doi.org/10.3390/en18030508.
[12] T. Selleri, A.D. Melas, A. Joshi, D. Manara, A. Perujo, R. Suarez-Bertoa, An overview of lean exhaust denox aftertreatment technologies and nox emission regulations in the european union, Catalysts 11 (2021), https://doi.org/10.3390/catal11030404.
[13] M. Piumetti, S. Bensaid, D. Fino, N. Russo, Catalysis in diesel engine NOx aftertreatment: a review, Catal. Struct. React. 1 (2015) 155–173, https://doi.org/10.1080/2055074X.2015.1105615.
[14] J. Wisniewska, M. Ziolek, N. Artioli, M. Daturi, The effect of niobium and tantalum on physicochemical and catalytic properties of silver and platinum catalysts based on MCF mesoporous cellular foams, J. Catal. 336 (2016) 58–74, https://doi.org/10.1016/j.jcat.2015.12.018.
[15] C. Coney, C. Hardacre, K. Morgan, N. Artioli, A.P.E. York, P. Millington, et al., Investigation of the oxygen storage capacity behaviour of three way catalysts using spatio-temporal analysis, Appl. Catal. B 258 (2019), https://doi.org/10.1016/j.apcatb.2019.117918.
[16] R. O'Donnell, K. Ralphs, M. Grolleau, H. Manyar, N. Artioli, Doping manganese oxides with ceria and ceria zirconia using a one-pot sol–gel method for low temperature diesel oxidation catalysts, Top. Catal. 63 (2020) 351–362, https://doi.org/10.1007/s11244-020-01250-x.
[17] M. Shen, L. Lv, J. Wang, J. Zhu, Y. Huang, J. Wang, Study of pt dispersion on ce based supports and the influence on the CO oxidation reaction, Chem. Eng. J. 255 (2014) 40–48, https://doi.org/10.1016/j.cej.2014.06.058.
[18] L. Castoldi, R. Matarrese, L. Kubiak, M. Daturi, N. Artioli, S. Pompa, et al., In-depth insights into N2O formation over Rh- and Pt-based LNT catalysts, Catal. Today 320 (2019) 141–151, https://doi.org/10.1016/j.cattod.2018.01.026.

[19] X. Liu, W. Ruettinger, X. Xu, R. Farrauto, Deactivation of Pt/CeO2 water-gas shift catalysts due to shutdown/startup modes for fuel cell applications, Appl. Catal. B 56 (2005) 69–75, https://doi.org/10.1016/j.apcatb.2004.04.026.
[20] C.I. Vignatti, M.S. Avila, C.R. Apesteguía, T.F. Garetto, Study of the water-gas shift reaction over pt supported on CeO 2-ZrO2 mixed oxides, Catal. Today 171 (2011) 297–303, https://doi.org/10.1016/j.cattod.2010.12.041.
[21] R.O. da Fonseca, G.S. Garrido, R.C. Rabelo-Neto, E.B. Silveira, R.C.C. Simões, L. V. Mattos, et al., Study of the effect of Gd-doping ceria on the performance of Pt/GdCeO2/Al2O3 catalysts for the dry reforming of methane, Catal. Today 355 (2020) 737–745, https://doi.org/10.1016/j.cattod.2019.04.079.
[22] J. Kim, Y. Ryou, T.H. Kim, G. Hwang, J. Bang, J. Jung, et al., Highly selective production of syngas (>99%) in the partial oxidation of methane at 480 °C over Pd/CeO2 catalyst promoted by HCl, Appl. Surf. Sci. (2021) 560, https://doi.org/10.1016/j.apsusc.2021.150043.
[23] P. Pantu, G.R. Gavalas, Methane partial oxidation on Pt/CeO 2 and Pt/Al 2 o 3 catalysts 223 (2002).
[24] Y.J. Mergler, A. Van Aalst, J. Van Delft, B.E. Nieuwenhuys, CO oxidation over promoted Pt catalysts, Appl. Catal. B: Environ. 10 (1996).
[25] U. Oran, D. Uner, Mechanisms of CO oxidation reaction and effect of chlorine ions on the CO oxidation reaction over Pt/CeO 2 and Pt/CeO 2/γ- al 2O 3 catalysts, Appl. Catal. B 54 (2004) 183–191, https://doi.org/10.1016/j.apcatb.2004.06.011.
[26] Z.K. Han, W. Liu, Y. Gao, Advancing the understanding of oxygen vacancies in ceria: insights into their formation, behavior, and catalytic roles, JACS Au (2025), https://doi.org/10.1021/jacsau.5c00095.
[27] R. Shyam, D. Negi, K. Shekhawat, F. Singh, S. Ojha, G.R. Umapathy, et al., Influence of 120 MeV au ion irradiation on phase transition, surface, and optical properties of Lead-Free (K,Na)NbO3 films, Physica Status Solidi (A) Appl. Mater. Sci. 220 (2023), https://doi.org/10.1002/pssa.202300179.
[28] Boris Navinšek, Sputtering-Surface changes induced by ion bombardment, Prog. Surf. Sci. 7 (1976) 49–70.
[29] V. Kumar, J. Prakash, D. Pathak, D.P. Sharma, L.P. Purohit, H.C. Swart, Ion beam engineering of implanted ZnO thin films for solar cell and lighting applications, Chem. Eng. J. Adv. 15 (2023), https://doi.org/10.1016/j.ceja.2023.100501.
[30] M. Niania, M. Sharpe, R. Webb, J.A. Kilner, The surface of complex oxides; ion beam based analysis of energy materials, Nucl. Instrum. Methods Phys. Res. B 480 (2020) 27–32, https://doi.org/10.1016/j.nimb.2020.07.022.
[31] A. Kumar, R. Devanathan, V. Shutthanandan, S.V.N.T. Kuchibhatla, A.S. Karakoti, Y. Yong, et al., Radiation-induced reduction of ceria in single and polycrystalline thin films, J. Phys. Chem. C. 116 (2012) 361–366, https://doi.org/10.1021/jp209345w.
[32] G.D. Wang, D.D. Kong, Y.H. Pan, H.B. Pan, J.F. Zhu, Low energy Ar-ion bombardment effects on the CeO 2 surface, Appl. Surf. Sci. 258 (2012) 2057–2061, https://doi.org/10.1016/j.apsusc.2011.04.103.
[33] K Ohler L., Scaglione S., Flori D., Riga J., Caudano R.. Ability of a gridless ion source to functionalize polypropylene surfaces by low-energy (60±100 eV) nitrogen ion bombardment. E¢ects of ageing in air and in water. n.d.
[34] L. Hanley, S.B. Sinnott, The growth and modification of materials via ion-surface processing, Surf. Sci. 500 (2002) 22, https://doi.org/10.1016/S0039-6028(01)01528-X.
[35] K. Fu, L. Zeng, J. Liu, M. Liu, S. Li, W. Guo, et al., Magnetron sputtering a high-performance catalyst for ultra-low-Pt loading PEMFCs, J. Alloy. Compd. 815 (2020), https://doi.org/10.1016/j.jallcom.2019.152374.
[36] Zlobin1 V.N., Bannikov2 M.G., Vasilev1 I.P., Cherkasov1 J.A., Gawrilenko1 P.N. Potential of use of ion implantation as a means of catalyst manufacturing. 2002.
[37] Kimata T., Kakitani K., Yamamoto S., Shimoyama I., Matsumura D., Iwase A., et al. Activity enhancement of platinum oxygen-reduction electrocatalysts using ion-beam induced defects. n.d.
[38] G. Colòn, M. Pijolat, F. Valdivieso, H. Vidal, J. Kaspar ", E. Finocchio, et al., Surface and structural characterization of CexZr1-xO2 CEZIRENCAT mixed oxides as potential three-way catalyst promoters, J. Chem. Soc. Faraday Trans. 94 (1998) 3717–3726, https://doi.org/10.1039/A807680D.
[39] T. Lesage, C. Verrier, P. Bazin, J. Saussey, M. Daturi, Studying the NOx-trap mechanism over a Pt-Rh/Ba/Al 2O3 catalyst by operando FT-IR spectroscopy, Phys. Chem. Chem. Phys. 5 (2003) 4435–4440, https://doi.org/10.1039/b305874n.
[40] Søren Birk Rasmussen, Susana Perez-Ferreras, Miguel A. Banares, M.D. Philippe Bazin, Does pelletizing catalysts influence the efficiency number of activity measurements? Spectrochemical engineering considerations for an accurate operando study, ACS Catal. 3 (2013) 86–94, https://doi.org/10.1021/cs300687v.
[41] C. Huang, W. Shan, Z. Lian, Y. Zhang, H. He, Recent advances in three-way catalysts of natural gas vehicles, 6407–19, Catal. Sci. Technol. 10 (2020), https://doi.org/10.1039/d0cy01320j.
[42] P. Fornasiero, G. Balducci, Kagpar J. Meriani, S. Di Monte, R. Graziani, M. Metal-loaded CeOz-ZrO 2 solid solutions as innovative catalysts for automotive catalytic converters 29 (1996).
[43] H.C. Yao, Y.F.Y. Yao, Ceria in automotive exhaust catalysts I, Oxygen Storage 86 (1984).
[44] C. Loschen, S.T. Bromley, K.M. Neyman, F. Illas, Understanding ceria nanoparticles from first-principles calculations, J. Phys. Chem. C 111 (2007) 10142–10145, https://doi.org/10.1021/jp072787m.
[45] M. Daturi, E. Finocchio, C. Binet, J.C. Lavalley, F. Fally, V. Perrichon, Study of bulk and surface reduction by hydrogen of CexZr1-xO2 mixed oxides followed by FTIR spectroscopy and magnetic balance, J. Phys. Chem. B 103 (1999) 4884–4891, https://doi.org/10.1021/jp9905981.
[46] O.U. Osazuwa, K.H. Ng, The roles of oxygen mobility and oxygen vacancy in metallic catalysts-prompted dry reforming of methane: a review, Renew. Energy 256 (2026), https://doi.org/10.1016/j.renene.2025.124074.
[47] A.H. Clark, H.R. Marchbank, D. Thompsett, J.M. Fisher, A. Longo, K.A. Beyer, et al., On the effect of metal loading on the reducibility and redox chemistry of ceria supported pd catalysts, Phys. Chem. Chem. Phys. 24 (2022) 2387–2395, https://doi.org/10.1039/d1cp04654c.
[48] B.R. Cuenya, Synthesis and catalytic properties of metal nanoparticles: size, shape, support, composition, and oxidation state effects, Thin Solid Films 518 (2010) 3127–3150, https://doi.org/10.1016/j.tsf.2010.01.018.
[49] J. Qu, W. Liu, R. Liu, J. He, D. Liu, Z. Feng, et al., Evolution of oxygen vacancies in cerium dioxide at atomic scale under CO2 reduction, Chem. Catal. 3 (2023), https://doi.org/10.1016/j.checat.2023.100759.
[50] D.C. Grinter, R. Ithnin, C.L. Pang, G. Thornton, Defect structure of ultrathin ceria films on Pt(111): atomic views from scanning tunnelling microscopy, J. Phys. Chem. C. 114 (2010) 17036–17041, https://doi.org/10.1021/jp102895k.
[51] I.P. Jain, G. Agarwal, Ion beam induced surface and interface engineering, Surf. Sci. Rep. 66 (2011) 77–172, https://doi.org/10.1016/j.surfrep.2010.11.001.
[52] IEEE Trans. Nucl. Sci. 28 (2) (1981) 1803–1807, n.d.
[53] J. Wang, E. Sauter, A. Nefedov, S. Heißler, F. Maurer, M. Casapu, et al., Dynamic structural evolution of Ceria-Supported pt particles: a thorough spectroscopic study, J. Phys. Chem. C 126 (2022) 9051–9058, https://doi.org/10.1021/acs.jpcc.2c02420.
[54] P. Magudapathy, S.K. Srivastava, P. Gangopadhyay, S. Amirthapandian, K. Saravanan, A. Das, et al., Alloying of metal nanoparticles by ion-beam induced sputtering, Chem. Phys. Lett. 667 (2017) 38–44, https://doi.org/10.1016/j.cplett.2016.11.041.